ESAIM: PROCEEDINGS, Vol. ?, 2009, 1-10
Editors: Will be set by the publisher

A HIGH-ORDER DISCONTINUOUS GALERKIN METHOD FOR THE SEISMIC WAVE PROPAGATION

Sarah Delcourte[1], Loula Fezoui[1] and Nathalie Glinsky-Olivier[2]

Abstract. We are interested in the simulation of P-SV seismic wave propagation by a high-order Discontinuous Galerkin method based on centered fluxes at the interfaces combined with a leap-frog time-integration. This non-diffusive method, previously developed for the Maxwell equations [4, 9, 20], is particularly well adapted to complex topographies and fault discontinuities in the medium. We prove that the scheme is stable under a CFL type condition and that a discrete energy is preserved on an infinite domain. Convergence properties and efficiency of the method are studied through numerical simulations in two and three dimensions of space.

Résumé. Nous nous intéressons à la propagation d'ondes sismiques de types P et SV par une méthode de Galerkin Discontinue d'ordre élevé basée sur des flux centrés aux interfaces combinés à un schéma saute-mouton en temps. Cette méthode non-dissipative, précédemment développée pour les équations de Maxwell [4, 9, 20], est particulièrement bien adaptée à des milieux présentant une topographie complexe ou contenant des failles. On prouve la stabilité du schéma sous une condition de type CFL ainsi que la conservation d'une energie discrète dans un domaine infini. L'efficacité de la méthode est illustrée par des simulations numériques en deux et trois dimensions d'espace.

1. Introduction

During an Earthquake, two types of waves are generated: body waves which travel through the interior of the Earth and surface waves which propagate just at the surface. In what follows, we focus on the body waves which can be distinguished into two types of waves: the P-waves (as primary waves because they arrive at first on a seismogram) and the S-waves (as secondary waves; their speed is lower than for the P-waves, so they appear later on a seismogram). The P-waves are longitudinal and compressive waves which alternatively compress or distend the ground in the direction of propagation. The S-waves are transverse and shear waves which displace the ground perpendicularly to the direction of propagation. More, their amplitude is often higher than those of the P-waves making them more destructive and we can note that fluids do not support shear stresses. The difference in the arrival time of the P and S-waves allows to specify the distance of an event.

The P-SV wave propagation in an isotropic, linearly elastic medium is modelised by the elastodynamic equations, which write initially in displacement-stress formulation; let be $\overline{U} = (U_\alpha)$, $\alpha = x, y, z$, the displacement

[1] INRIA, NACHOS project-team, 2004 route des Lucioles, BP 93, 06902 Sophia Antipolis.
[2] CERMICS and INRIA, NACHOS project-team, 2004 route des Lucioles, BP 93, 06902 Sophia Antipolis.
{Sarah.Delcourte, Loula.Fezoui, Nathalie.Glinsky}@inria.fr

vector and $\overline{\overline{\sigma}} = (\sigma_{\alpha,\beta})$, $\alpha, \beta = x, y, z$, the stress tensor, then the system reads

$$\left\{ \begin{array}{rcl} \rho \, \dfrac{\partial^2 \overline{U}}{\partial t^2} & = & \nabla \cdot \overline{\overline{\sigma}} \, , \\ \overline{\overline{\sigma}} & = & \lambda \, (\nabla \cdot \overline{U}) \, \overline{\overline{I}} + \mu \, (\boldsymbol{\nabla} \overline{U} + (\boldsymbol{\nabla} \overline{U})^T) \, , \end{array} \right. \tag{1}$$

where $\overline{\overline{I}}$ is the identity matrix, ρ is the density of the medium and λ and μ are the Lamé constants.

Using the Helmholtz decomposition of $\overline{U} = \boldsymbol{\nabla}\phi + \boldsymbol{\nabla} \times \overline{\psi} = \overline{U}_p + \overline{U}_s$ and properties of the operators, we can establish the following identity:

$$\boldsymbol{\nabla} \left(\frac{\partial^2 \phi}{\partial t^2} - v_p^2 \, \Delta \phi \right) + \boldsymbol{\nabla} \times \left(\frac{\partial^2 \overline{\psi}}{\partial t^2} - v_s^2 \, \boldsymbol{\Delta} \overline{\psi} \right) = 0 \, , \tag{2}$$

where $v_p = \sqrt{\frac{\lambda + 2\mu}{\rho}}$ and $v_s = \sqrt{\frac{\mu}{\rho}}$ are the velocities of the P and S-waves respectively, and $v_p > v_s$. One solution of (2) can be obtained by setting both bracketed terms to zero. This yields two wave equations, one for each potential ϕ and $\overline{\psi}$, which correspond to the P and S-waves:

$$\frac{\partial^2 \phi}{\partial t^2} - v_p^2 \, \Delta \phi = 0 \quad \text{and} \quad \frac{\partial^2 \overline{\psi}}{\partial t^2} - v_s^2 \, \boldsymbol{\Delta} \overline{\psi} = 0 \, . \tag{3}$$

In order to solve the problem (1), we introduce the velocity vector $\overline{V} = \dfrac{\partial \overline{U}}{\partial t}$ in (1) and we obtain the velocity-stress formulation, which allows to take into account more easily the boundary conditions:

$$\left\{ \begin{array}{rcl} \rho \, \dfrac{\partial \overline{V}}{\partial t} & = & \nabla \cdot \overline{\overline{\sigma}} \, , \\ \dfrac{\partial \overline{\overline{\sigma}}}{\partial t} & = & \lambda \, (\nabla \cdot \overline{V}) \, \overline{\overline{I}} + \mu \, (\boldsymbol{\nabla} \overline{V} + (\boldsymbol{\nabla} \overline{V})^T) \, . \end{array} \right. \tag{4}$$

The most famous method to solve this problem is the finite difference scheme of Virieux [22] which can be viewed as an adaptation to elastodynamic equations of the Yee's scheme [23], very popular in electromagnetism. This method is very easy to implement, second order accurate, not too costly in CPU time and weakly dispersive, but the major drawback is the restriction to rectangular grids, not suited for geometrical irregularities. This method has known later many extensions in three dimensions, to anisotropic media or to higher order of accuracy for example. Some other methods have been further developed such as the finite element methods which have allowed to deal with meshes adapted to complex geometries. However, they are very costly because, at each time-step, one needs to invert a N-diagonal mass matrix with N depending on the order of the method and the dimension of the space. This difficulty was overcome by the use of Gauss-Lobatto Legendre quadrature formulae and these methods applied to quadrangular or hexahedral meshes are referenced as spectral element methods [14].

In what follows, we focus on Discontinuous Galerkin methods which are finite element methods with discontinuities at the interfaces, well adapted to take into account cracks in the medium. They are non-conforming methods (in the sense of finite elements), so that we can note a greater flexibility (compared to spectral element methods) in the choice of the local degree p of the polynomial interpolation. They require in general the use of numerical fluxes, as for the finite volume methods. These methods have been introduced in 1973 by Reed & Hill to simulate neutron transport. The first analysis of the method for hyperbolic equations has been presented by Lesaint & Raviart [16, 17] in 1974. Their result has been further improved and the analysis substantially

broadened by Johnson, Pitkaränta & Nävert [11,12], who have established that the optimal order of convergence in the L^2-norm is $p+\frac{1}{2}$ if polynomials of degree p are used. These methods have only become popular since the 90s with several remarkable contributions as Cockburn et al. [5] who studied the non-linear hyperbolic equations combined to a Discontinuous Galerkin discretization in space with an explicit Runge-Kutta method in time. This renewed interest can be explained by the capability of the Discontinuous Galerkin methods to adapt to most meshes such as unstructured and non-conforming meshes. Moreover, we can note their flexibility in the use of high-order *hp*-adaptive finite element methods which consist in techniques of mesh refinement (h-adaptivity) and in the variation of the degree p of the polynomial interpolation (p-adaptivity); see, for example, Süli et al. [21] or Demkowicz et al. [7].

For the seismic wave propagation, Käser et al. [8, 13] have been recently interested in the development of high-order Discontinuous Galerkin method. They combine upwind fluxes through the interfaces with the ADER scheme in time, so that they get the same order of accuracy in space and in time. However, their scheme is diffusive. It is the reason why we propose here centered fluxes through the interfaces with a leap-frog time-discretization, which leads to a non-dissipative combination. The extension to higher order in space is realized by Lagrange interpolants, locally on triangles (in two dimensions) or on tetraedra (in three dimensions), which do not necessitate the inversion of a global mass matrix. This method can be viewed as a generalization of the finite volume method developed in [1] and allows the use of unstructured and non-conforming meshes, well adapted to heterogeneities of the medium and to complex topographies.

This article is organized as follows. In section 2, we state the velocity-stress formulation in a symmetrical pseudo-conservative form. Then, in section 3, we detail the discretization of the equations system by the Discontinuous Galerkin method based on centered fluxes in space and a leap-frog scheme in time. The approximation of the boundary conditions is also presented. After, we study, in section 4, some properties of the scheme and finally, in section 5, we illustrate this study by some numerical results in two and three dimensions in space on two types of meshes. Convergence and efficiency of the method are addressed.

2. Velocity-stress formulation in pseudo-conservative form

We note $\overline{\mathbb{W}} = \left(\overline{V}, \overline{\sigma}\right)^T$ the vector composed by the velocity components $\overline{V} = (V_x, V_y, V_z)^T$ and the stress components $\overline{\sigma} = (\sigma_{xx}, \sigma_{yy}, \sigma_{zz}, \sigma_{xy}, \sigma_{xz}, \sigma_{yz})^T$. Then, the system (4) can be rewritten as

$$\frac{\partial \overline{\mathbb{W}}}{\partial t} + \sum_{\alpha \in \{x,y,z\}} \overline{\overline{A}}_\alpha \left(\rho, \lambda, \mu\right) \; \partial_\alpha \overline{\mathbb{W}} = 0 \,. \tag{5}$$

Moreover, for any real vector $\overline{n} = (n_x, n_y, n_z)^T$, we define the matrix

$$\overline{\overline{A}}_n(\rho, \lambda, \mu) = \sum_{\alpha \in \{x,y,z\}} \overline{\overline{A}}_\alpha(\rho, \lambda, \mu) \; n_\alpha \,, \tag{6}$$

which reads:

$$\overline{\overline{A}}_n(\rho, \lambda, \mu) = -\begin{pmatrix} 0 & 0 & 0 & \frac{n_x}{\rho} & 0 & 0 & \frac{n_y}{\rho} & \frac{n_z}{\rho} & 0 \\ 0 & 0 & 0 & 0 & \frac{n_y}{\rho} & 0 & \frac{n_x}{\rho} & 0 & \frac{n_z}{\rho} \\ 0 & 0 & 0 & 0 & 0 & \frac{n_z}{\rho} & 0 & \frac{n_x}{\rho} & \frac{n_y}{\rho} \\ (\lambda+2\mu)n_x & \lambda n_y & \lambda n_z & 0 & 0 & 0 & 0 & 0 & 0 \\ \lambda n_x & (\lambda+2\mu)n_y & \lambda n_z & 0 & 0 & 0 & 0 & 0 & 0 \\ \lambda n_x & \lambda n_y & (\lambda+2\mu)n_z & 0 & 0 & 0 & 0 & 0 & 0 \\ \mu n_y & \mu n_x & 0 & 0 & 0 & 0 & 0 & 0 & 0 \\ \mu n_z & 0 & \mu n_x & 0 & 0 & 0 & 0 & 0 & 0 \\ 0 & \mu n_z & \mu n_y & 0 & 0 & 0 & 0 & 0 & 0 \end{pmatrix} \tag{7}$$

Remark that the matrices $\overline{\overline{A}}_\alpha(\rho,\lambda,\mu)$, for $\alpha \in \{x,y,z\}$, are easily deduced from the expression of $\overline{\overline{A}}_n(\rho,\lambda,\mu)$ by keeping only one component n_α equal to 1 while the two other are equal to zero. We choose here not to detail these matrices.

In order to express the system (5) in pseudo conservative form, we introduce the following change of variables $\overline{\tilde{\sigma}} = \overline{\overline{R}}\,\overline{\sigma}$ on the stress components. For example in 3D

$\overline{\overline{R}} = \begin{pmatrix} \frac{1}{3} & \frac{1}{3} & \frac{1}{3} & 0 & 0 & 0 \\ \frac{2}{3} & -\frac{1}{3} & -\frac{1}{3} & 0 & 0 & 0 \\ -\frac{1}{3} & \frac{2}{3} & -\frac{1}{3} & 0 & 0 & 0 \\ 0 & 0 & 0 & 1 & 0 & 0 \\ 0 & 0 & 0 & 0 & 1 & 0 \\ 0 & 0 & 0 & 0 & 0 & 1 \end{pmatrix}$. So, the system reads

$$\overline{\overline{\Lambda}}(\rho,\lambda,\mu)\,\frac{\partial \overline{\tilde{\mathbb{W}}}}{\partial t} + \sum_{\alpha\in\{x,y,z\}} \overline{\overline{\tilde{A}}}_\alpha\,\partial_\alpha \overline{\tilde{\mathbb{W}}} = 0\,, \tag{8}$$

where $\overline{\tilde{\mathbb{W}}} = \left(\overline{V}, \overline{\tilde{\sigma}}\right)^T$ and $\overline{\overline{\Lambda}} = diag\left(\rho,\rho,\rho,\frac{3}{3\lambda+2\mu},\frac{3}{2\mu},\frac{3}{2\mu},\frac{1}{\mu},\frac{1}{\mu},\frac{1}{\mu}\right)$ is a diagonal matrix containing the characteristics of the medium. We can notice that now the matrices $\overline{\overline{\tilde{A}}}_\alpha$ are constant and do not depend anymore on the material properties.

At last, we multiply the previous system by the following matrix $\overline{\overline{S}}_0 = \begin{pmatrix} 1 & 0 & 0 & 0 & 0 & 0 & 0 & 0 & 0 \\ 0 & 1 & 0 & 0 & 0 & 0 & 0 & 0 & 0 \\ 0 & 0 & 1 & 0 & 0 & 0 & 0 & 0 & 0 \\ 0 & 0 & 0 & 1 & 0 & 0 & 0 & 0 & 0 \\ 0 & 0 & 0 & 0 & \frac{2}{3} & \frac{1}{3} & 0 & 0 & 0 \\ 0 & 0 & 0 & 0 & \frac{1}{3} & \frac{2}{3} & 0 & 0 & 0 \\ 0 & 0 & 0 & 0 & 0 & 0 & 1 & 0 & 0 \\ 0 & 0 & 0 & 0 & 0 & 0 & 0 & 1 & 0 \\ 0 & 0 & 0 & 0 & 0 & 0 & 0 & 0 & 1 \end{pmatrix}$ in order to obtain a symmetrical system. Therefore, we finally get the symmetrical pseudo-conservative formulation:

$$\overline{\overline{\Lambda}}_0(\rho,\lambda,\mu)\,\frac{\partial \overline{\tilde{\mathbb{W}}}}{\partial t} + \sum_{\alpha\in\{x,y,z\}} \overline{\overline{S}}_\alpha\,\partial_\alpha \overline{\tilde{\mathbb{W}}} = 0\,, \tag{9}$$

where $\overline{\overline{\Lambda}}_0 = \overline{\overline{S}}_0\overline{\overline{\Lambda}}$ and $\overline{\overline{S}}_\alpha = \overline{\overline{S}}_0\overline{\overline{\tilde{A}}}_\alpha$ $(\alpha = x,y,z)$ are symmetric. This formulation will be very useful to establish the energy conservation. For the numerical simulations, we add boundary conditions on the free surface $\overline{\overline{\sigma}}\,\overline{n} = 0$ or absorbing conditions to approximate an infinite domain.

3. Discretization

We consider a polygonal domain Ω, discretized in N_T symplectic elements $\mathcal{T}_i$ (triangles in 2D and tetrahedra in 3D), which form a partition of the domain. We denote by $\mathcal{V}(i)$ the set of indices of the neighboring elements of $\mathcal{T}_i$ and we note S_{ik} each internal face common to both elements $\mathcal{T}_i$ and $\mathcal{T}_k$ i.e. $S_{ik} = \mathcal{T}_i \cap \mathcal{T}_k$. Finally, some elements $\mathcal{T}_i$ have one or more faces common to the boundary of the domain. The set of the indices k of such faces $S_k^{b_i} = \mathcal{T}_i \cap \partial\Omega$ is denoted by $\mathcal{E}(i)$. Remark that this set is empty for most elements.

We multiply each equation of the problem (4) by a scalar test function $\phi_l^{\mathcal{T}_i}$ and we integrate them on each element $\mathcal{T}_i$:

$$\int_{\mathcal{T}_i} \left[\frac{\partial \overline{\mathbb{W}}}{\partial t} + \sum_{\alpha \in \{x,y,z\}} \overline{\overline{A}}_\alpha(\rho,\lambda,\mu)\ \partial_\alpha \overline{\mathbb{W}} \right] \phi_l^{\mathcal{T}_i}\ dxdydz = 0\,. \tag{10}$$

Then, we assume that the characteristics of the medium (ρ,λ,μ) are constant over each element $\mathcal{T}_i$ and we apply the Green formula to the second term of (10):

$$\int_{\mathcal{T}_i} \frac{\partial \overline{\mathbb{W}}}{\partial t}\ \phi_l^{\mathcal{T}_i}\ dxdydz - \sum_{\alpha \in \{x,y,z\}} \overline{\overline{A}}_\alpha^{\mathcal{T}_i} \int_{\mathcal{T}_i} \overline{\mathbb{W}}\ \partial_\alpha \phi_l^{\mathcal{T}_i}\ dxdydz + \overline{\overline{A}}_n^{\mathcal{T}_i} \int_{\partial \mathcal{T}_i} \overline{\mathbb{W}}\ \phi_l^{\mathcal{T}_i}\ ds = 0\,, \tag{11}$$

where $\overline{\overline{A}}_n^{\mathcal{T}_i}$ is the restriction of $\overline{\overline{A}}_n$ to the element $\mathcal{T}_i$ and $\overline{n}$ represents the outwards unit normal vector to $\mathcal{T}_i$. Now, we take as test function the Lagrange nodal interpolants $\phi_l^{\mathcal{T}_i}$ of $\mathcal{P}_m(\mathcal{T}_i)$, set of polynomials with a degree m. Then, each component W of the vector $\overline{\mathbb{W}}$ is approximated on $\mathcal{T}_i$ by:

$$W_{|_{\mathcal{T}_i}}(x,y,z,t) = \sum_{j=1}^{ndof} W_j^{\mathcal{T}_i}(t)\ \phi_j^{\mathcal{T}_i}(x,y,z)\,, \tag{12}$$

where $ndof$ is the number of degrees of freedom on the element $\mathcal{T}_i$ and $\phi_j^{\mathcal{T}_i}$ $(j = 1, ..., ndof)$ are the associated basis functions. The first term of (11) can be expressed by:

$$\forall l = 1, ..., ndof\,, \qquad \int_{\mathcal{T}_i} \frac{\partial}{\partial t} \overline{\mathbb{W}}\ \phi_l^{\mathcal{T}_i}\ dxdydz = \sum_{j=1}^{ndof} \overline{\overline{M}}_{lj}^{\mathcal{T}_i} \frac{d}{dt} \overline{\mathbb{W}}_j^{\mathcal{T}_i}\,, \tag{13}$$

where $\overline{\overline{M}}^{\mathcal{T}_i} = \left(\int_{\mathcal{T}_i} \phi_j^{\mathcal{T}_i}\ \phi_l^{\mathcal{T}_i}\ dxdydz \right)_{1 \le j,l \le ndof}$ denotes the mass matrix on the element $\mathcal{T}_i$.
The second integral of (11) is approximated in the following way:

$$\forall l = 1, ..., ndof\,, \qquad \sum_{\alpha \in \{x,y,z\}} \overline{\overline{A}}_\alpha^{\mathcal{T}_i} \int_{\mathcal{T}_i} \overline{\mathbb{W}}\ \partial_\alpha \phi_l^{\mathcal{T}_i}\ dxdydz = \sum_{\alpha \in \{x,y,z\}} \overline{\overline{A}}_\alpha^{\mathcal{T}_i} \sum_{j=1}^{ndof} \overline{\overline{G}}_{\alpha,lj}^{\mathcal{T}_i}\ \overline{\mathbb{W}}_j^{\mathcal{T}_i}\,, \tag{14}$$

with $\overline{\overline{G}}_\alpha^{\mathcal{T}_i} = \left(\int_{\mathcal{T}_i} \phi_j^{\mathcal{T}_i}\ \partial_\alpha \phi_l^{\mathcal{T}_i}\ dxdydz \right)_{1 \le j,l \le ndof}$. Then, to calculate the integral on $\partial \mathcal{T}_i$, we split this boundary in internal and boundary faces:

$$\forall l = 1, ..., ndof\,, \qquad \overline{\overline{A}}_n^{\mathcal{T}_i} \sum_{k \in \mathcal{V}(i)} \int_{S_{ik}} \overline{\mathbb{W}}\ \phi_l^{\mathcal{T}_i}\ ds + \overline{\overline{A}}_n^{\mathcal{T}_i} \sum_{k \in \mathcal{E}(i)} \int_{S_k^{b_i}} \overline{\mathbb{W}}\ \phi_l^{\mathcal{T}_i}\ ds. \tag{15}$$

For the interior faces S_{ik}, we apply centered fluxes by introducing the mean value on this face:

$$\overline{\mathbb{W}}_{|_{S_{ik}}} = \frac{1}{2} \left(\overline{\mathbb{W}}^{\mathcal{T}_i} + \overline{\mathbb{W}}^{\mathcal{T}_k} \right)\,. \tag{16}$$

Therefore, this integral writes

$$\forall l = 1, ..., ndof\,, \qquad \overline{\overline{A}}_n^{\mathcal{T}_i} \sum_{k \in \mathcal{V}(i)} \int_{S_{ik}} \overline{\mathbb{W}}\ \phi_l^{\mathcal{T}_i}\ ds = \frac{1}{2}\ \overline{\overline{A}}_n^{\mathcal{T}_i} \sum_{k \in \mathcal{V}(i)} \sum_{j=1}^{ndof} \left[\left(\overline{\overline{R}}_{|_{S_{ik}}}^{\mathcal{T}_i} \right)_{lj} \overline{\mathbb{W}}_j^{\mathcal{T}_i} + \left(\overline{\overline{R}}_{|_{S_{ik}}}^{\mathcal{T}_k} \right)_{lj} \overline{\mathbb{W}}_j^{\mathcal{T}_k} \right]\,, \tag{17}$$

where we have set $\overline{\overline{R}}^{\mathcal{T}_i}_{|_{S_{ik}}} = \left(\int_{S_{ik}} \phi_j^{\mathcal{T}_i} \phi_l^{\mathcal{T}_i} \, ds \right)_{1 \leq j,l \leq ndof}$ and $\overline{\overline{R}}^{\mathcal{T}_k}_{|_{S_{ik}}} = \left(\int_{S_{ik}} \phi_j^{\mathcal{T}_k} \phi_l^{\mathcal{T}_i} \, ds \right)_{1 \leq j,l \leq ndof}$.

For the boundary integrals, two type of boundary conditions have been considered : a free surface condition at the physical interface between air and the medium, and an absorbing condition on the artificial boundaries of an infinite domain.

Free surfaces: On these faces, we compute the fluxes by introducing weakly the condition $\overline{\overline{\sigma}}\,\overline{n} = 0$ in the second term of (15). No special condition is applied on the velocity. So, for a boundary face $S_k^{b_i}$ of $\mathcal{T}_i$, this integral reduces to

$$\forall l = 1, ..., ndof\,, \quad \overline{\overline{A}}_n^{\mathcal{T}_i} \int_{S_k^{b_i}} \overline{\mathbb{W}} \; \phi_l^{\mathcal{T}_i} \, ds = \overline{\overline{A}}_n^{\mathcal{T}_i} \sum_{j=1}^{ndof} \left(\overline{\overline{R}}^{\mathcal{T}_i}_{|_{S_k^{b_i}}} \right)_{lj} \left(\overline{\mathbb{W}}^{\mathcal{T}_i}_{|_{S_k^{b_i}}} \right)_j , \tag{18}$$

where $\overline{\mathbb{W}}^{\mathcal{T}_i}_{|_{S_k^{b_i}}} = (V_x^{\mathcal{T}_i}, V_y^{\mathcal{T}_i}, V_z^{\mathcal{T}_i}, 0, 0, 0, 0, 0, 0)^T$ and $\overline{\overline{R}}^{\mathcal{T}_i}_{|_{S_k^{b_i}}} = \left(\int_{S_k^{b_i}} \phi_j^{\mathcal{T}_i} \phi_l^{\mathcal{T}_i} \, ds \right)_{1 \leq j,l \leq ndof}$.

Absorbing surfaces: To simulate infinite domains, we introduce artificial boundaries, chosen such that the solution is inside the computational domain and sufficiently far of the frontier, and we impose absorbing conditions.

For any real unit vector $\overline{n} = (n_x, n_y, n_z)^T \neq 0_{\mathbb{R}^3}$, the matrix $\overline{\overline{A}}_n$ of (6) is diagonalizable in $\mathbb{R}$, ie all its eigenvalues λ_k (k=1,...,9) are real:

$$\lambda_1 = -v_p, \quad \lambda_2 = \lambda_3 = -v_s, \quad \lambda_4 = \lambda_5 = \lambda_6 = 0, \quad \lambda_7 = \lambda_8 = v_s, \quad \lambda_9 = v_p\,,$$

and we note $\overline{\overline{P}}$ the matrix whose column k is the right eigenvector associated to the eigenvalue λ_k. The absorbing boundary conditions are then dealt with an upwind technique where we consider only the outgoing waves. For that, we write $\overline{\overline{A}}_n = \overline{\overline{A}}_n^+ + \overline{\overline{A}}_n^-$ where we set $\overline{\overline{A}}_n^+ = \overline{\overline{P}}\;\overline{\overline{\Lambda^+}}\;\overline{\overline{P}}^{-1}$ and $\overline{\overline{A}}_n^- = \overline{\overline{P}}\;\overline{\overline{\Lambda^-}}\;\overline{\overline{P}}^{-1}$ with $\overline{\overline{\Lambda^+}} = diag\{(\lambda_k^+)_{1 \leq k \leq 9}\}$ and $\overline{\overline{\Lambda^-}} = diag\{(\lambda_k^-)_{1 \leq k \leq 9}\}$ the diagonal matrices composed by the positive $\lambda_k^+ = \max(\lambda_k, 0)$ and the negative $\lambda_k^- = \min(\lambda_k, 0)$ eigenvalues of $\overline{\overline{A}}_n$. Then, for a boundary face $S_k^{b_i}$ of $\mathcal{T}_i$, the second integral of (15) is approximated by:

$$\forall l = 1, ..., ndof\,, \quad \overline{\overline{A}}_n^{\mathcal{T}_i} \int_{S_k^{b_i}} \overline{\mathbb{W}} \; \phi_l^{\mathcal{T}_i} \, ds = \overline{\overline{A}}_n^{\mathcal{T}_i +} \sum_{j=1}^{ndof} \left(\overline{\overline{R}}^{\mathcal{T}_i}_{|_{S_k^{b_i}}} \right)_{lj} \overline{\mathbb{W}}_j^{\,\mathcal{T}_i} . \tag{19}$$

It is a first-order approximation, efficient for waves with a normal incidence to the artificial boundaries.

At last, we apply a leap-frog time-integration scheme. It is a two step explicit scheme which allows, combined to the centered fluxes defined at (16)-(17), to get a non-diffusive scheme. We note Δt the time-step and we can view the final scheme on each element $\mathcal{T}_i$ by introducing discrete operators $\mathcal{F}_\alpha^{\mathcal{T}_i}$ $(\alpha = x, y, z)$ and $\mathcal{G}_{\alpha,\beta}^{\mathcal{T}_i}$ $(\alpha, \beta = x, y, z)$ which collect the integrals on $\mathcal{T}_i$ and $\partial\mathcal{T}_i$:

$$\overline{\overline{M}}^{\mathcal{T}_i} \, \frac{\overline{\mathcal{W}_{V_\alpha}^{n+1}} - \overline{\mathcal{W}_{V_\alpha}^{n}}}{\Delta t} = \overline{\mathcal{F}_\alpha^{\mathcal{T}_i} \left(\overline{V}^n, \overline{\sigma}^{n+\frac{1}{2}} \right)}, \tag{20}$$

$$\overline{\overline{M}}^{\mathcal{T}_i} \, \frac{\overline{\mathcal{W}_{\sigma_{\alpha\beta}}^{n+\frac{3}{2}}} - \overline{\mathcal{W}_{\sigma_{\alpha\beta}}^{n+\frac{1}{2}}}}{\Delta t} = \overline{\mathcal{G}_{\alpha,\beta}^{\mathcal{T}_i} \left(\overline{V}^{n+1}, \overline{\sigma}^{n+\frac{1}{2}} \right)}, \tag{21}$$

where $\overline{\mathcal{W}_{V_\alpha}}$ and $\overline{\mathcal{W}_{\sigma_{\alpha\beta}}}$ are respectively the vectors composed by the $ndof$ values of V_α $(\alpha = x, y, z)$ and $\sigma_{\alpha\beta}$ $(\alpha, \beta = x, y, z)$ in the element $\mathcal{T}_i$, $\overline{V}^{n+1}$ represents the velocity at $(n+1)\Delta t$ and $\overline{\sigma}^{n+\frac{1}{2}}$ the stress tensor at

$(n+\frac{1}{2})\Delta t$.
Note that the initialisation is realized at $t=t_0$ for the velocity and at $t=t_0+\frac{\Delta t}{2}$ for the stress tensor.

4. Properties of the scheme

4.1. VF scheme on cubic elementary volumes

Thanks to standard techniques, the following properties for the P0 scheme (finite volumes: VF) on a domain discretized by parallelepipedic elementary volumes are easy to state:

- First, the scheme is second order consistant in space and in time.
- Then, applying Fourier analysis, we can prove that the scheme is stable under the following optimal CFL condition:
$$v_p\ \Delta t\ \sqrt{\frac{1}{\Delta x^2}+\frac{1}{\Delta y^2}+\frac{1}{\Delta z^2}} \leq 2\ , \tag{22}$$
where $\Delta x, \Delta y$ and Δz are the standard notations for the lengths of the parallelepipeds in the three directions.
- Using the Lax theorem, the scheme converges with a second order accuracy to the solution of the elastodynamics problem on meshes composed of parallelepipeds when (22) is satisfied.
- For the longitudinal or compressional wave, the dispersion relation $\omega^2=|k_p|^2\ v_p^2$ is deduced from the scalar wave equation of (3), whereas for transverse or shear waves, it is deduced from the vectorial wave equation of (3) and we have $\omega^2=|k_s|^2\ v_s^2$, where ω is the pulsation and, $k_p=(k_{x_p},k_{y_p},k_{z_p})^T$ and $k_s=(k_{x_s},k_{y_s},k_{z_s})^T$ are the wave number vectors associated to the P and SV-waves respectively (by convention, $|k|^2=k_x^2+k_y^2+k_z^2$).

The numerical dispersion relations for the P and SV-waves are given with an order two:

$$\omega^2\left[1-\frac{w^2\Delta t^2}{12}+O\left(w^4\Delta t^4\right)\right] = |k_p|^2\ v_p^2\left[1-\frac{k_{x_p}^4\Delta x^2+k_{y_p}^4\Delta y^2+k_{z_p}^4\Delta z^2}{3\,|k_p|^2}+O\left(\frac{k_{x_p}^6\Delta x^4+k_{y_p}^6\Delta y^4+k_{z_p}^6\Delta z^4}{|k_p|^2}\right)\right],$$
$$\omega^2\left[1-\frac{w^2\Delta t^2}{12}+O\left(w^4\Delta t^4\right)\right] = |k_s|^2\ v_s^2\left[1-\frac{k_{x_s}^4\Delta x^2+k_{y_s}^4\Delta y^2+k_{z_s}^4\Delta z^2}{3\,|k_s|^2}+O\left(\frac{k_{x_s}^6\Delta x^4+k_{y_s}^6\Delta y^4+k_{z_s}^6\Delta z^4}{|k_s|^2}\right)\right].$$

Remark 4.1. : on a twice as fine grid $\left(\frac{\Delta x}{2},\frac{\Delta y}{2},\frac{\Delta z}{2}\right)$, the optimal CFL condition and the numerical dispersion error of the VF scheme are the same that those obtained with the finite difference scheme of Virieux [22] on a grid $(\Delta x,\Delta y,\Delta z)$. These results are similar to those described by Remaki in [19,20] for the Maxwell equations discretized by centered fluxes through the interfaces combined with a leap-frog time-integration.

4.2. Discrete energy

In order to keep the proof simple, we choose to study the discrete energy only in the 2D case, but it can be easily extended to the 3D equations. Such a study in both 2D and 3D cases, but leading to a very restrictive stability condition can be found in [2]. We define the discrete energy E^n at time $n\Delta t$ by:

$$E^n = \frac{1}{2}\sum_{i=1}^{N_T}\int_{\mathcal{T}_i}\left[\rho\ (V_{x\,i}^{\ n})^2+\rho\ (V_{y\,i}^{\ n})^2+\frac{1}{\lambda+\mu}\ \tilde{\sigma}_{xx\,i}^{\ n+1/2}\ \tilde{\sigma}_{xx\,i}^{\ n-1/2}\right.$$
$$\left.+\ \frac{1}{\mu}\ \tilde{\sigma}_{yy\,i}^{\ n+1/2}\ \tilde{\sigma}_{yy\,i}^{\ n-1/2}+\frac{1}{\mu}\ \tilde{\sigma}_{zz\,i}^{\ n+1/2}\ \tilde{\sigma}_{zz\,i}^{\ n-1/2}\right]. \tag{23}$$

Theorem 4.2. *On an infinite domain, the discrete elastodynamic energy is preserved through one time-step:*

$$\forall n \in \mathbb{N}^*, \quad E^{n+1} = E^n \,,$$

which means the scheme is non-diffusive.

Proof. In the two dimensional case, Eq. (9) can be rewritten as:

$$\left\{ \begin{array}{rl} \rho \dfrac{\partial \overline{V}}{\partial t} = & \displaystyle\sum_{\alpha \in \{x,y\}} \partial_\alpha \overline{\overline{M}}_\alpha \overline{\tilde{\sigma}} \,, \\ \overline{\overline{\Lambda}}_{\tilde{\sigma}}(\lambda,\mu) \ \dfrac{\partial \overline{\tilde{\sigma}}}{\partial t} = & \displaystyle\sum_{\alpha \in \{x,y\}} \partial_\alpha \overline{\overline{N}}_\alpha \overline{V} \,, \end{array} \right. \tag{24}$$

with $\overline{\overline{M}}_x = \overline{\overline{N}}_x^T = \begin{pmatrix} 1 & 1 & 0 \\ 0 & 0 & 1 \end{pmatrix}$, $\overline{\overline{M}}_y = \overline{\overline{N}}_y^T = \begin{pmatrix} 0 & 0 & 1 \\ 1 & -1 & 0 \end{pmatrix}$ and $\overline{\overline{\Lambda}}_{\tilde{\sigma}} = diag\left(\dfrac{1}{\lambda+\mu}, \dfrac{1}{\mu}, \dfrac{1}{\mu}\right)$ is a diagonal matrix containing the Lamé constants λ and μ associated to the stress vector $\overline{\tilde{\sigma}} = \left(\dfrac{\sigma_{xx}+\sigma_{yy}}{2}, \dfrac{\sigma_{xx}-\sigma_{yy}}{2}, \sigma_{xy}\right)^T$.

In what follows, we calculate the variation of the discrete energy during one time-step Δt:

$$E^{n+1} - E^n = \sum_{i=1}^{N_T} \left[\rho \int_{\mathcal{T}_i} \frac{\overline{V}_i^{n+1} + \overline{V}_i^n}{2} \cdot \left(V_i^{n+1} - V_i^n\right) + \int_{\mathcal{T}_i} \frac{\overline{\tilde{\sigma}}_i^{n+\frac{1}{2}}}{2} \overline{\overline{\Lambda}}_{\tilde{\sigma}} \left(\overline{\tilde{\sigma}}_i^{n+\frac{3}{2}} - \overline{\tilde{\sigma}}_i^{n-\frac{1}{2}} \right) \right] . \tag{25}$$

We define $\overline{V}_i^{\left[n+\frac{1}{2}\right]} = \dfrac{\overline{V}_i^{n+1} + \overline{V}_i^n}{2}$ and the previous equation becomes:

$$\begin{aligned} E^{n+1} - E^n \ = \ \Delta t \sum_{i=1}^{N_T} \Bigg[& - \sum_{\alpha \in \{x,y\}} \int_{\mathcal{T}_i} \left(\partial_\alpha \overline{V}_i^{\left[n+\frac{1}{2}\right]} \right)^T \overline{\overline{M}}_\alpha \ \overline{\tilde{\sigma}}_i^{n+\frac{1}{2}} + \frac{1}{2} \sum_{k \in \mathcal{V}(i)} \int_{S_{ik}} \left(\overline{V}_i^{\left[n+\frac{1}{2}\right]} \right)^T \overline{\overline{M}}_\alpha \left(\overline{\tilde{\sigma}}_i^{n+\frac{1}{2}} + \overline{\tilde{\sigma}}_k^{n+\frac{1}{2}} \right) \ n_{\alpha_{ik}} \\ & - \sum_{\alpha \in \{x,y\}} \int_{\mathcal{T}_i} \left(\partial_\alpha \overline{\tilde{\sigma}}_i^{n+\frac{1}{2}} \right)^T \overline{\overline{N}}_\alpha \ \overline{V}_i^{\left[n+\frac{1}{2}\right]} + \frac{1}{2} \sum_{k \in \mathcal{V}(i)} \int_{S_{ik}} \left(\overline{\tilde{\sigma}}_i^{n+\frac{1}{2}} \right)^T \overline{\overline{N}}_\alpha \left(\overline{V}_i^{\left[n+\frac{1}{2}\right]} + \overline{V}_k^{\left[n+\frac{1}{2}\right]} \right) \ n_{\alpha_{ik}} \Bigg] \,, \end{aligned} \tag{26}$$

where $n_{\alpha_{ik}}$ $(\alpha = x, y)$ are the components of the unit normal vector oriented from $\mathcal{T}_i$ to $\mathcal{T}_k$.

As $\overline{\overline{M}}_\alpha = \overline{\overline{N}}_\alpha^T$ $(\alpha = x, y)$, we easily check that $\left(\overline{V}_i^{\left[n+\frac{1}{2}\right]} \right)^T \ \overline{\overline{M}}_\alpha \ \partial_\alpha \overline{\tilde{\sigma}}_i^{n+\frac{1}{2}} = \left(\partial_\alpha \overline{\tilde{\sigma}}_i^{n+\frac{1}{2}} \right)^T \overline{\overline{N}}_\alpha \ \overline{V}_i^{\left[n+\frac{1}{2}\right]}$ and then, the Green formula implies that:

$$\int_{\mathcal{T}_i} \left(\partial_\alpha \overline{V}_i^{\left[n+\frac{1}{2}\right]} \right)^T \overline{\overline{M}}_\alpha \ \overline{\tilde{\sigma}}_i^{n+\frac{1}{2}} + \int_{\mathcal{T}_i} \left(\partial_\alpha \overline{\tilde{\sigma}}_i^{n+\frac{1}{2}} \right)^T \overline{\overline{N}}_\alpha \ \overline{V}_i^{\left[n+\frac{1}{2}\right]} = \sum_{k \in \mathcal{V}(i)} \int_{S_{ik}} \left(\overline{V}_i^{\left[n+\frac{1}{2}\right]} \right)^T \overline{\overline{M}}_\alpha \ \overline{\tilde{\sigma}}_i^{n+\frac{1}{2}} \ n_{\alpha_{ik}} \,. \tag{27}$$

Therefore, introducing the previous equation in (26), the variation of the discrete energy can be rewritten as:

$$E^{n+1} - E^n = \frac{\Delta t}{2} \sum_{i=1}^{N_T} \sum_{k \in \mathcal{V}(i)} \left[\int_{S_{ik}} \left(\overline{V}_i^{\left[n+\frac{1}{2}\right]} \right)^T \overline{\overline{M}}_\alpha \ \overline{\tilde{\sigma}}_k^{n+\frac{1}{2}} \ n_{\alpha_{ik}} + \sum_{k \in \mathcal{V}(i)} \int_{S_{ik}} \left(\overline{\tilde{\sigma}}_i^{n+\frac{1}{2}} \right)^T \overline{\overline{N}}_\alpha \ \overline{V}_k^{\left[n+\frac{1}{2}\right]} \ n_{\alpha_{ik}} \right] . \tag{28}$$

Finally, the two terms of $E^{n+1} - E^n$ vanish on the internal edges thanks to the orientation of $n_{\alpha_{ik}}$ from $\mathcal{T}_i$ to $\mathcal{T}_k$, which means that the discrete elastodynamic energy is preserved in an infinite domain. □

In what follows, we note $\|W\|_{\mathcal{T}_i}$ and $\|W\|_{S_{ik}}$ the L^2-norms of a component W of $\overline{\overline{\mathbb{W}}}$ over the element $\mathcal{T}_i$ and the face S_{ik} respectively.

Moreover, for any element $\mathcal{T}_i$, we assume that there exists two constants a_i and b_{ik} ($k \in \mathcal{V}(i)$) such that:

$$\forall W \in \mathcal{P}_m(\mathcal{T}_i), \begin{cases} \forall \alpha \in \{x,y,z\}, & \|\partial_\alpha W\|_{\mathcal{T}_i} \leq \dfrac{a_i |S_i|}{|\mathcal{T}_i|} \|W\|_{\mathcal{T}_i}, \\ \forall k \in \mathcal{V}(i), & \|W\|_{S_{ik}} \leq \sqrt{\dfrac{b_{ik}\,|S_{ik}|}{|\mathcal{T}_i|}}\, \|W\|_{\mathcal{T}_i}, \end{cases} \tag{29}$$

where $|S_{ik}|$ is the length of the edge S_{ik} and $|S_i| = \sum_{k\in\mathcal{V}(i)} |S_{ik}|$ (resp. $|\mathcal{T}_i|$) is the perimeter (resp. the area) of the element $\mathcal{T}_i$.

On the other hand, there exist two integers C_1 and C_2 such that:

$$\sum_{i=1}^{N_T} \sum_{k\in\mathcal{V}(i)} \|V_{\alpha_k} n_{x_{ik}}\|^2_{T_k} \leq C_1 \sum_{i=1}^{N_T} \|V_{\alpha_i}\|^2_{T_i}, \tag{30}$$

$$\sum_{i=1}^{N_T} \sum_{k\in\mathcal{V}(i)} \|V_{\alpha_k} n_{y_{ik}}\|^2_{T_k} \leq C_2 \sum_{i=1}^{N_T} \|V_{\alpha_i}\|^2_{T_i}. \tag{31}$$

Remark that C_1 and C_2 are bounded by the number of faces of the element T_i (ie three for triangles, in 2D). In the case of a reference triangle $\widehat{T} = ((0,0),(1,0),(0,1))$, thanks to the orientation of the normal vector $\overline{n}$ to the edges, n_x or n_y can vanish and then $C_1 = C_2 = 2$.

Theorem 4.3. *On an infinite domain, using the scheme described in section 3, under the assumptions (29), the discrete elastodynamic energy (23) is preserved through iterations and is a positive definite quadratic form for all the unknowns of $\overline{\overline{\mathbb{W}}}$. Therefore, the scheme is L^2-stable under the CFL conditions:*

$$\forall i = 1,...,N_T, \quad \rho - (\lambda+3\mu)\,\Delta t^2\,\frac{a_i^2|S_i|^2}{|\mathcal{T}_i|^2} - \frac{\Delta t^2}{4}\left(\max_{i=1,\dots,N_T} \sum_{k\in\mathcal{V}(i)} \frac{b_{ik}^2|S_{ik}|^2}{|\mathcal{T}_i||\mathcal{T}_k|}\right)(C_1(\lambda+\mu)+C_2\mu) \geq 0, \tag{32}$$

$$\forall i = 1,...,N_T, \quad \rho - (\lambda+3\mu)\,\Delta t^2\,\frac{a_i^2|S_i|^2}{|\mathcal{T}_i|^2} - \frac{\Delta t^2}{4}\left(\max_{i=1,\dots,N_T} \sum_{k\in\mathcal{V}(i)} \frac{b_{ik}^2|S_{ik}|^2}{|\mathcal{T}_i||\mathcal{T}_k|}\right)(C_2(\lambda+\mu)+C_1\mu) \geq 0, \tag{33}$$

where C_1 and C_2 are the two integers defined in (30) and (31) respectively.

Proof. At first, we integrate on an element $\mathcal{T}_i$ the third equation of (24) multiplied by a function test ϕ in $\mathcal{P}_m(\mathcal{T}_i)$. Applying the procedures of discretization described in section 3, we get:

$$\begin{aligned} \frac{1}{\lambda+\mu}\int_{\mathcal{T}_i} \frac{\tilde{\sigma}_{xx\,i}^{\,n+1/2} - \tilde{\sigma}_{xx\,i}^{\,n-1/2}}{\Delta t}\,\phi\,dxdydz &= -\int_{\mathcal{T}_i}\left(V_x^n\,\frac{\partial\phi}{\partial x} + V_y^n\,\frac{\partial\phi}{\partial y}\right)dxdydz \\ &+ \frac{1}{2}\sum_{k\in\mathcal{V}(i)}\int_{S_{ik}}\left[\left(V_{x_i}^n + V_{x_k}^n\right)n_{x_{ik}} + \left(V_{y_i}^n + V_{y_k}^n\right)n_{y_{ik}}\right]\phi\,ds \end{aligned} \tag{34}$$

We can split the boundary integrals into two integrals by respect to the indices i and k. Then, we apply the Green formula to those dealing with the couple (V_{x_i}, V_{y_i}):

$$\frac{1}{2}\sum_{k\in\mathcal{V}(i)}\int_{S_{ik}}\left[V_{x_i}^n\ n_{x_{ik}}+V_{y_i}^n\ n_{y_{ik}}\right]\phi\ ds=\frac{1}{2}\int_{\mathcal{T}_i}\left[\frac{\partial V_{x_i}^n}{\partial x}\ \phi+V_{x_i}^n\ \frac{\partial\phi}{\partial x}+\frac{\partial V_{y_i}^n}{\partial y}\ \phi+V_{y_i}^n\ \frac{\partial\phi}{\partial y}\right]\ dxdydz\,.$$

So, substituting the previous line in (34) with $\phi=\tilde{\sigma_{xx}}_i^{n-1/2}$ and applying the Cauchy-Schwarz inequality, we get for $T_3=\dfrac{1}{\lambda+\mu}\displaystyle\int_{\mathcal{T}_i}\tilde{\sigma_{xx}}_i^{n+1/2}\tilde{\sigma_{xx}}_i^{n-1/2}$:

$$\begin{aligned}
T_3 \ &\geq\ \frac{1}{\lambda+\mu}\left\|\tilde{\sigma_{xx}}_i^{n-1/2}\right\|_{\mathcal{T}_i}^2-\frac{\Delta t}{2}\sum_{k\in\mathcal{V}(i)}\left\|V_{x_k}^n n_{x_{ik}}+V_{y_k}^n n_{y_{ik}}\right\|_{S_{ik}}\ \left\|\tilde{\sigma_{xx}}_i^{n-1/2}\right\|_{S_{ik}}\\
&-\ \frac{\Delta t}{2}\left[\left\|\frac{\partial V_{x_i}^n}{\partial x}\right\|_{\mathcal{T}_i}\ \left\|\tilde{\sigma_{xx}}_i^{n-1/2}\right\|_{\mathcal{T}_i}+\left\|\frac{\partial V_{y_i}^n}{\partial y}\right\|_{\mathcal{T}_i}\ \left\|\tilde{\sigma_{xx}}_i^{n-1/2}\right\|_{\mathcal{T}_i}\right.\\
&\qquad\left.+\left\|V_{x_i}^n\right\|_{\mathcal{T}_i}\ \left\|\frac{\partial\tilde{\sigma_{xx}}_i^{n-1/2}}{\partial x}\right\|_{\mathcal{T}_i}+\left\|V_{y_i}^n\right\|_{\mathcal{T}_i}\ \left\|\frac{\partial\tilde{\sigma_{xx}}_i^{n-1/2}}{\partial y}\right\|_{\mathcal{T}_i}\right]\,.
\end{aligned}$$

Then, applying the assumptions (29) and expressing the previous line as a sum of square terms, we obtain:

$$\begin{aligned}
T_3 \ &\geq\ \frac{1}{\lambda+\mu}\left[\left\|\tilde{\sigma_{xx}}_i^{n-1/2}\right\|_{\mathcal{T}_i}\right.\\
&\qquad\left.-\frac{\Delta t}{2}(\lambda+\mu)\left[\frac{a_i|S_i|}{|\mathcal{T}_i|}\left(\left\|V_{x_i}^n\right\|_{\mathcal{T}_i}+\left\|V_{y_i}^n\right\|_{\mathcal{T}_i}\right)+\frac{1}{2}\sum_{k\in\mathcal{V}(i)}\frac{b_{ik}\ |S_{ik}|}{\sqrt{|\mathcal{T}_i||\mathcal{T}_k|}}\left\|V_{x_k}^n n_{x_{ik}}+V_{y_k}^n n_{y_{ik}}\right\|_{T_k}\right]\right]^2\\
-\ &(\lambda+\mu)\frac{\Delta t^2}{4}\left[\frac{a_i|S_i|}{|\mathcal{T}_i|}\left(\left\|V_{x_i}^n\right\|_{\mathcal{T}_i}+\left\|V_{y_i}^n\right\|_{\mathcal{T}_i}\right)+\frac{1}{2}\sum_{k\in\mathcal{V}(i)}\frac{b_{ik}\ |S_{ik}|}{\sqrt{|\mathcal{T}_i||\mathcal{T}_k|}}\left\|V_{x_k}^n n_{x_{ik}}+V_{y_k}^n n_{y_{ik}}\right\|_{T_k}\right]^2\,.
\end{aligned}$$

We focus on the second term of T_3 and we apply twice an inequality of type $(a+b)^2\leq 2\ (a^2+b^2)$ and the Cauchy-Schwarz inequality, so that we obtain:

$$\begin{aligned}
T_3 \ &\geq\ \frac{1}{\lambda+\mu}\left[\left\|\tilde{\sigma_{xx}}_i^{n-1/2}\right\|_{\mathcal{T}_i}\right.\\
&\qquad\left.-\frac{\Delta t}{2}(\lambda+\mu)\left[\frac{a_i|S_i|}{|\mathcal{T}_i|}\left(\left\|V_{x_i}^n\right\|_{\mathcal{T}_i}+\left\|V_{y_i}^n\right\|_{\mathcal{T}_i}\right)+\frac{1}{2}\sum_{k\in\mathcal{V}(i)}\frac{b_{ik}\ |S_{ik}|}{\sqrt{|\mathcal{T}_i||\mathcal{T}_k|}}\left\|V_{x_k}^n n_{x_{ik}}+V_{y_k}^n n_{y_{ik}}\right\|_{T_k}\right]\right]^2\\
-\ &(\lambda+\mu)\frac{\Delta t^2}{2}\left[2\frac{a_i^2|S_i|^2}{|\mathcal{T}_i|^2}\left(\left\|V_{x_i}^n\right\|_{\mathcal{T}_i}^2+\left\|V_{y_i}^n\right\|_{\mathcal{T}_i}^2\right)+\frac{1}{4}\sum_{k\in\mathcal{V}(i)}\frac{b_{ik}^2\ |S_{ik}|^2}{|\mathcal{T}_i||\mathcal{T}_k|}\sum_{k\in\mathcal{V}(i)}\left\|V_{x_k}^n n_{x_{ik}}+V_{y_k}^n n_{y_{ik}}\right\|_{T_k}^2\right]\,.
\end{aligned}$$

Proceeding in the very same way for the fourth term $T_4 = \frac{1}{\mu}\int_{\mathcal{T}_i} \tilde{\sigma}_{yy}{}_i^{n+1/2}\,\tilde{\sigma}_{yy}{}_i^{n-1/2}$ of the discrete energy (23), we find:

$$\begin{aligned} T_4 \;\geq\; & \frac{1}{\mu}\left[\left\|\tilde{\sigma}_{yy}{}_i^{n-1/2}\right\|_{\mathcal{T}_i}\right. \\ & \left. -\frac{\Delta t}{2}\mu\left[\frac{a_i|S_i|}{|\mathcal{T}_i|}\left(\left\|V_{x_i}^n\right\|_{\mathcal{T}_i}+\left\|V_{y_i}^n\right\|_{\mathcal{T}_i}\right)+\frac{1}{2}\sum_{k\in\mathcal{V}(i)}\frac{b_{ik}\,|S_{ik}|}{\sqrt{|\mathcal{T}_i||\mathcal{T}_k|}}\left\|V_{x_k}^n n_{x_{ik}}-V_{y_k}^n n_{y_{ik}}\right\|_{T_k}\right]\right]^2 \\ - \;\; & \mu\frac{\Delta t^2}{2}\left[2\frac{a_i^2|S_i|^2}{|\mathcal{T}_i|^2}\left(\left\|V_{x_i}^n\right\|_{\mathcal{T}_i}^2+\left\|V_{y_i}^n\right\|_{\mathcal{T}_i}^2\right)+\frac{1}{4}\sum_{k\in\mathcal{V}(i)}\frac{b_{ik}^2\,|S_{ik}|^2}{|\mathcal{T}_i||\mathcal{T}_k|}\sum_{k\in\mathcal{V}(i)}\left\|V_{x_k}^n n_{x_{ik}}-V_{y_k}^n n_{y_{ik}}\right\|_{T_k}^2\right], \end{aligned}$$

and for the fifth term $T_5 = \frac{1}{\mu}\int_{\mathcal{T}_i} \tilde{\sigma}_{xy}{}_i^{n+1/2}\,\tilde{\sigma}_{xy}{}_i^{n-1/2}$, we get:

$$\begin{aligned} T_5 \;\geq\; & \frac{1}{\mu}\left[\left\|\tilde{\sigma}_{xy}{}_i^{n-1/2}\right\|_{\mathcal{T}_i}\right. \\ & \left. -\frac{\Delta t}{2}\mu\left[\frac{a_i|S_i|}{|\mathcal{T}_i|}\left(\left\|V_{x_i}^n\right\|_{\mathcal{T}_i}+\left\|V_{y_i}^n\right\|_{\mathcal{T}_i}\right)+\frac{1}{2}\sum_{k\in\mathcal{V}(i)}\frac{b_{ik}\,|S_{ik}|}{\sqrt{|\mathcal{T}_i||\mathcal{T}_k|}}\left\|V_{y_k}^n n_{x_{ik}}+V_{x_k}^n n_{y_{ik}}\right\|_{T_k}\right]\right]^2 \\ - \;\; & \mu\frac{\Delta t^2}{2}\left[2\frac{a_i^2|S_i|^2}{|\mathcal{T}_i|^2}\left(\left\|V_{x_i}^n\right\|_{\mathcal{T}_i}^2+\left\|V_{y_i}^n\right\|_{\mathcal{T}_i}^2\right)+\frac{1}{4}\sum_{k\in\mathcal{V}(i)}\frac{b_{ik}^2\,|S_{ik}|^2}{|\mathcal{T}_i||\mathcal{T}_k|}\sum_{k\in\mathcal{V}(i)}\left\|V_{y_k}^n n_{x_{ik}}+V_{x_k}^n n_{y_{ik}}\right\|_{T_k}^2\right]. \end{aligned}$$

When we sum T_3, T_4 and T_5, we are lead to add three terms containing the real number b_{ik}. Therefore, applying (30) and (31), we remark that

$$\begin{aligned} & \sum_{i=1}^{N_T}\sum_{k\in\mathcal{V}(i)}\left[(\lambda+\mu)\left\|V_{x_k}^n n_{x_{ik}}+V_{y_k}^n n_{y_{ik}}\right\|_{T_k}^2+\mu\left\|V_{x_k}^n n_{x_{ik}}-V_{y_k}^n n_{y_{ik}}\right\|_{T_k}^2+\mu\left\|V_{y_k}^n n_{x_{ik}}+V_{x_k}^n n_{y_{ik}}\right\|_{T_k}^2\right] \\ & \leq \sum_{i=1}^{N_T}\left[2(\lambda+\mu)\left(C_1\sum_{i=1}^{N_T}\left\|V_{x_i}^n\right\|_{T_i}^2+C_2\sum_{i=1}^{N_T}\left\|V_{y_i}^n\right\|_{T_i}^2\right)+2\mu\left(C_2\sum_{i=1}^{N_T}\left\|V_{x_i}^n\right\|_{T_i}^2+C_1\sum_{i=1}^{N_T}\left\|V_{y_i}^n\right\|_{T_i}^2\right)\right]. \end{aligned}$$

Finally, the discrete elastodynamic energy at $n\Delta t$ is bounded lower in the following way:

$$
\begin{aligned}
E^n \;\geq\; & \frac{1}{2}\sum_{i=1}^{N_T}\frac{1}{\lambda+\mu}\left[\left\|\tilde{\sigma}_{xx}{}_i^{n-1/2}\right\|_{\mathcal{T}_i}\right. \\
& \left.-\frac{\Delta t}{2}(\lambda+\mu)\left[\frac{a_i|S_i|}{|\mathcal{T}_i|}\left(\left\|V_{x_i}^n\right\|_{\mathcal{T}_i}+\left\|V_{y_i}^n\right\|_{\mathcal{T}_i}\right)+\frac{1}{2}\sum_{k\in\mathcal{V}(i)}\frac{b_{ik}\;|S_{ik}|}{\sqrt{|\mathcal{T}_i||\mathcal{T}_k|}}\left\|V_{x_k}^n n_{x_{ik}}+V_{y_k}^n n_{y_{ik}}\right\|_{T_k}\right]\right]^2 \\
+ \;& \frac{1}{2}\sum_{i=1}^{N_T}\frac{1}{\mu}\left[\left\|\tilde{\sigma}_{yy}{}_i^{n-1/2}\right\|_{\mathcal{T}_i}\right. \\
& \left.-\frac{\Delta t}{2}\mu\left[\frac{a_i|S_i|}{|\mathcal{T}_i|}\left(\left\|V_{x_i}^n\right\|_{\mathcal{T}_i}+\left\|V_{y_i}^n\right\|_{\mathcal{T}_i}\right)+\frac{1}{2}\sum_{k\in\mathcal{V}(i)}\frac{b_{ik}\;|S_{ik}|}{\sqrt{|\mathcal{T}_i||\mathcal{T}_k|}}\left\|V_{x_k}^n n_{x_{ik}}-V_{y_k}^n n_{y_{ik}}\right\|_{T_k}\right]\right]^2 \\
+ \;& \frac{1}{2}\sum_{i=1}^{N_T}\frac{1}{\mu}\left[\left\|\tilde{\sigma}_{xy}{}_i^{n-1/2}\right\|_{\mathcal{T}_i}\right. \\
& \left.-\frac{\Delta t}{2}\mu\left[\frac{a_i|S_i|}{|\mathcal{T}_i|}\left(\left\|V_{x_i}^n\right\|_{\mathcal{T}_i}+\left\|V_{y_i}^n\right\|_{\mathcal{T}_i}\right)+\frac{1}{2}\sum_{k\in\mathcal{V}(i)}\frac{b_{ik}\;|S_{ik}|}{\sqrt{|\mathcal{T}_i||\mathcal{T}_k|}}\left\|V_{y_k}^n n_{x_{ik}}+V_{x_k}^n n_{y_{ik}}\right\|_{T_k}\right]\right]^2 \\
+ \;& \frac{1}{2}\sum_{i=1}^{N_T}\left[\rho-(\lambda+3\mu)\;\Delta t^2\;\frac{a_i^2|S_i|^2}{|\mathcal{T}_i|^2}-\frac{\Delta t^2}{8}\left(\max_{i=1,\ldots,N_T}\sum_{k\in\mathcal{V}(i)}\frac{b_{ik}^2\;|S_{ik}|^2}{|\mathcal{T}_i||\mathcal{T}_k|}\right)(2C_1(\lambda+\mu)+2C_2\mu)\right]\left\|V_{x_i}^n\right\|_{\mathcal{T}_i}^2 \\
+ \;& \frac{1}{2}\sum_{i=1}^{N_T}\left[\rho-(\lambda+3\mu)\;\Delta t^2\;\frac{a_i^2|S_i|^2}{|\mathcal{T}_i|^2}-\frac{\Delta t^2}{8}\left(\max_{i=1,\ldots,N_T}\sum_{k\in\mathcal{V}(i)}\frac{b_{ik}^2\;|S_{ik}|^2}{|\mathcal{T}_i||\mathcal{T}_k|}\right)(2C_2(\lambda+\mu)+2C_1\mu)\right]\left\|V_{y_i}^n\right\|_{\mathcal{T}_i}^2,
\end{aligned}
$$

and we can conclude that E^n is a positive quadratic form of all the unknowns V_α^n and $\sigma_{\alpha,\beta}^{n-\frac{1}{2}}$ if (32) and (33) are satisfied $\forall i = 1, ..., N_T$. □

Remark 4.4. The stability conditions (32) and (33) on Δt are sufficient conditions and may be suboptimal. Indeed, in the particular case of the finite volumes (P_0 polynomial approximation), we have clearly $\forall i, a_i = 0$ and $\forall i, \forall k \in \mathcal{V}(i),\ b_{ik} = 1$. For domains partitioned with reference triangles (where h is the smallest altitude) or squares (where h is the longest edge), we have $C_1 = C_2 = 2$ and we obtain from (32) and (33) the following CFL conditions:

$$v_p\frac{\Delta t}{h} \leq \frac{1}{\sqrt{2}} \quad \text{for squares} \quad \text{and} \quad v_p\frac{\Delta t}{h} \leq \frac{1}{2} \quad \text{for reference triangles.}$$

However, the Cauchy-Schwarz inequalities are strong majorations and using exclusively the finite volume scheme, i.e. without integral, we are able, with similar ideas to the previous proof, to obtain the optimal CFL conditions:

$$v_p\frac{\Delta t}{h} \leq \sqrt{2} \quad \text{for squares} \quad \text{and} \quad v_p\frac{\Delta t}{h} \leq 1 \quad \text{for reference triangles.}$$

5. Numerical results

5.1. **Limit of stability**

In order to check numerically the stability of the method, we apply the numerical scheme (20)-(21) in the two dimensional case. The domain of computation is the unit square and we introduce an explosive point source at the center $(x_s, y_s) = (0.5, 0.5)$ of Ω. This source is added as a right-hand side of the system (4), only for the

diagonal components of the stress tensor σ_{xx} and σ_{yy} and this source term is $\delta(x_s, y_s)\, s(t)$ where δ is the Dirac measure and $s(t)$ is a Ricker function whose expression is $s(t) = \left[-1 + 2\alpha(t-t_0)^2\right] \exp^{-\alpha(t-t_0)^2}$ with $t_0 = 0.3$ and $\alpha = 1.0$. We impose free surface boundary conditions on all sides of domain and we set adimensional values for the medium properties $\rho = 1.0$, $\lambda = 0.5$ and $\mu = 0.25$, which implies that $v_p = 1$ and $v_s = 0.5$.

The Dirac measure has the nice property to group together all the frequences, so that we are ensured to get the more restrictive CFL condition in this case. (To prove this affirmation, we can check that the support of the Fourier transform of a Dirac measure is $\mathbb{R}$ whereas the support of the Fourier transform of an harmonic e^{ix} is reduced to a singleton). Initial conditions for the system are $\overline{V} = 0$ and $\overline{\sigma} = 0$. Energy is brought only by the source for $t \in [0; 2.5]$. For times greater than 2.5s, the source does not provide energy anymore to the system, so that it is preserved if the scheme is stable. The time-step used for the calculation depends on geometrical properties of the mesh and is proportional to a cfl value which is a data of the simulation. An optimal formula for the time-step would provide a stable scheme until the value $cfl = 1$ in the finite volume case. For unstructured meshes, such a formula is not easily established. To test the stability of the scheme, two different meshes have been used : an uniform mesh composed of 800 right triangles and an unstructured mesh constructed via a mesher depending on the number of points on each side of the domain (here 21 points). A mesh step h is defined, it is the length of the smallest altitude of the mesh.

On figures 1 and 2, we display the limit of stability of the scheme for both meshes that is the evolution of energy as a function of time for different values of cfl. Different methods have been tested ; the notation Pk refers to a method based on polynomials of degree k. When studying the figure 1 for the structured mesh, we notice than for the P0 method, the scheme is stable until a value of $cfl = 1.0$. For higher order methods, the scheme is stable for lower time-steps. The value of cfl is about 0.37 for the P1 method, 0.2 for the P2 method, 0.13 for the P3 method and 0.09 for the P4 method. In all cases, when the scheme is stable, the energy is preserved for times greater than 2.5s. For the unstructured mesh, figure 2, we remark than P0 scheme allows cfl values until 1.376 which proves that the time-step formula is non optimal and too restrictive in this case. For this mesh, the cfl value allowing stability is also decreasing as the order of the method increases and conservation of the energy is verified.

5.2. **Monodimensional pulse**

The second problem we have studied is the propagation of a monodimensional pulse. Although this is a one dimensional problem, it is possible to solve it using the two-dimensional solver. The initial condition for the impulsion is:

$$\left\{ \begin{array}{rcl} V_x(x, t_0 = 0) & = & \exp^{-50(x-x_0)^2}, \\ \sigma_{xx}(x, t_0 = 0) & = & -\exp^{-50(x-x_0)^2}, \end{array} \right. \tag{35}$$

and for all t, we assume $V_y = 0$ and $\sigma_{yy} = \sigma_{xy} = 0$. The analytical solution in 1D is calculated using the characteristic method according to the initial condition at $t_0 = 0$. Its expression is:

$$\left\{ \begin{array}{rcl} V_x(t,x) & = & \dfrac{1}{2}\left[V_x(0, x - v_p\ t) - \dfrac{\sigma_{xx}(0, x - v_p\ t)}{\rho\ v_p}\right] \\ & + & \dfrac{1}{2}\left[V_x(0, x + v_p\ t) + \dfrac{\sigma_{xx}(0, x + v_p\ t)}{\rho\ v_p}\right], \\ \sigma_{xx}(t,x) & = & \dfrac{1}{2}\ \rho\ v_p\ \left[V_x(0, x + v_p\ t) + \dfrac{\sigma_{xx}(0, x + v_p\ t)}{\rho\ v_p}\right] \\ & - & \dfrac{1}{2}\ \rho\ v_p\ \left[V_x(0, x - v_p\ t) - \dfrac{\sigma_{xx}(0, x - v_p\ t)}{\rho\ v_p}\right]. \end{array} \right. \tag{36}$$

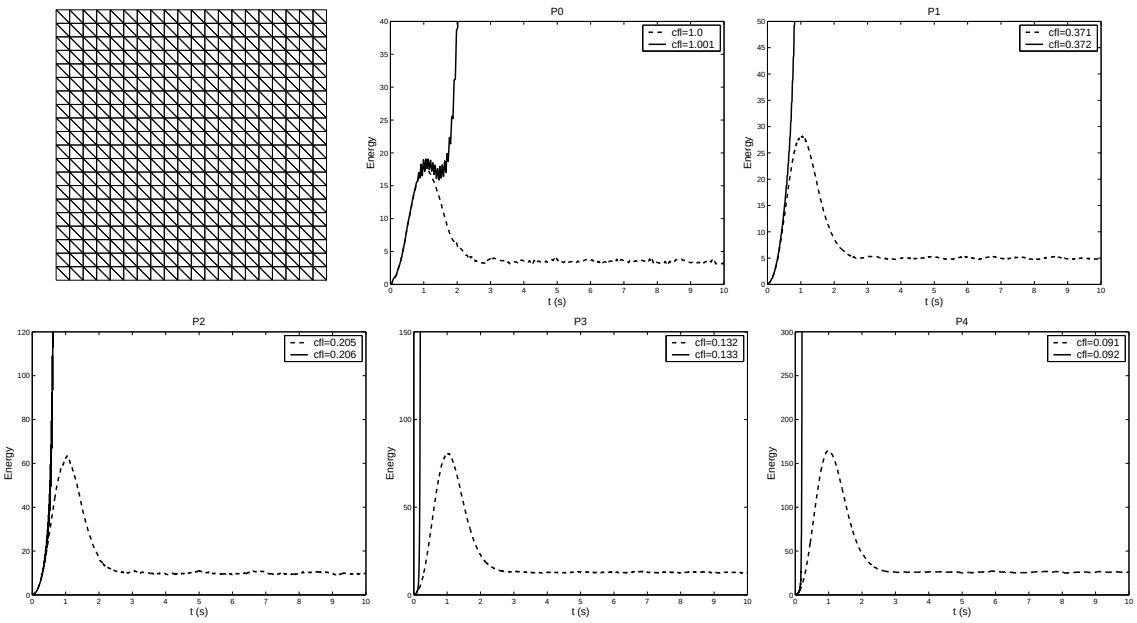

FIGURE 1. Evolution of the energy by respect to the time for the uniform mesh.

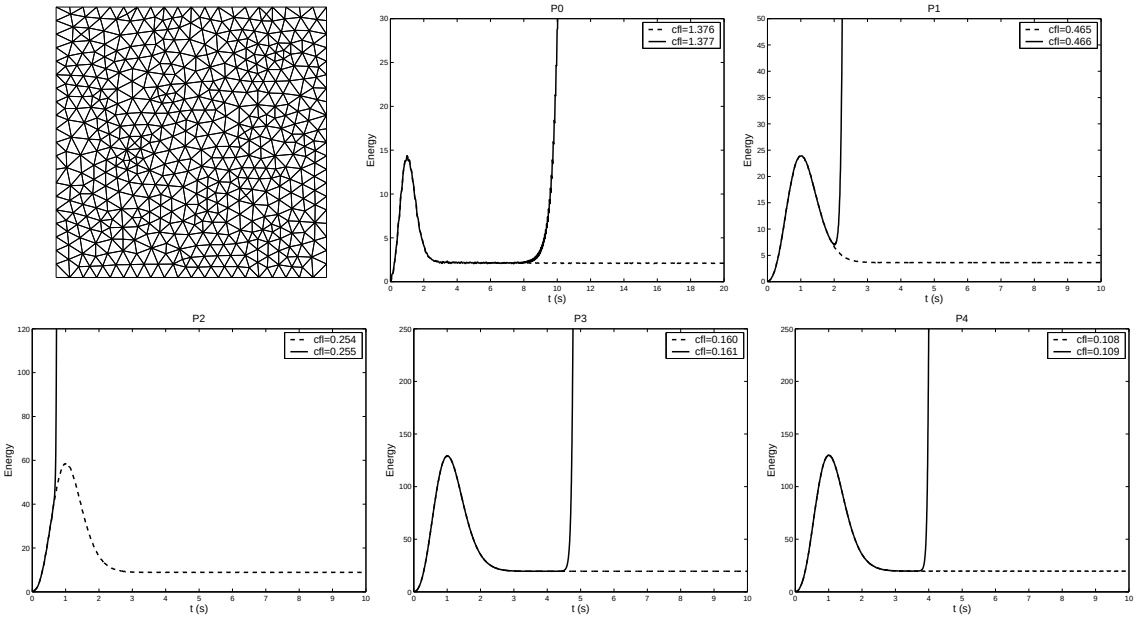

FIGURE 2. Evolution of the energy by respect to the time for the unstructured mesh.

The domain of computation is $[0,2]^2$ on which we apply absorbing boundary conditions. As previously, we set dimensionless values for $\rho = 1.0$, $\lambda = 0.5$ and $\mu = 0.25$, then the P and S-wave velocities are respectively

$v_p = 1$ and $v_s = 1/2$. The pulse is placed in the middle of the domain ($x_0 = 1.$) and the initialisation of the leap-frog scheme is realized by taking the values at $t = 0$ for the velocity components and at $t = \frac{\Delta t}{2}$ for the stress components. Note that in 2D, the matrix

$$\overline{\overline{A}}_n(\rho,\lambda,\mu) = \sum_{\alpha\in\{x,y\}} \overline{\overline{A}}_\alpha(\rho,\lambda,\mu)\ n_\alpha\,, \tag{37}$$

is diagonalizable in $\mathbb{R}$, ie all its eigenvalues are real:

$$\lambda_1 = -v_p,\quad \lambda_2 = -v_s,\quad \lambda_3 = 0,\quad \lambda_4 = v_s,\quad \lambda_5 = v_p\,,$$

and the associated eigenvectors form a basis of $\mathbb{R}^5$ and are the columns of the following matrix:

$$\overline{\overline{P}} = \begin{pmatrix} v_p\ n_x & -v_s\ n_y & 0 & v_s\ n_y & -v_p\ n_x \\ v_p\ n_y & v_s\ n_x & 0 & -v_s\ n_x & -v_p\ n_y \\ \lambda+2\mu\ n_x^2 & -2\mu\ n_x\ n_y & n_y^2 & -2\mu\ n_x\ n_y & \lambda+2\mu\ n_x^2 \\ \lambda+2\mu\ n_y^2 & 2\mu\ n_x\ n_y & n_x^2 & 2\mu\ n_x\ n_y & \lambda+2\mu\ n_y^2 \\ 2\mu\ n_x\ n_y & \mu\ (n_x^2-n_y^2) & -n_x\ n_y & \mu\ (n_x^2-n_y^2) & 2\mu\ n_x\ n_y \end{pmatrix}.$$

We remind the boundary condition on the absorbing edges

$$\overline{\overline{A}}_n^{\mathcal{T}_i} \int_{S_k^{b_i}} \overline{\mathbb{W}}\ \phi_l^{\mathcal{T}_i}\ ds = \overline{\overline{A}}_n^{\mathcal{T}_i+} \sum_{j=1}^{ndof} \left(R^{\mathcal{T}_i}_{|_{S_k^{b_i}}}\right)_{lj} \overline{\mathbb{W}}_j^{\mathcal{T}_i} = \overline{\overline{P}}_{|_{S_k^{b_i}}}\ \overline{\overline{\Lambda^+}}^{\mathcal{T}_i}\ \overline{\overline{P}}^{-1}_{|_{S_k^{b_i}}} \sum_{j=1}^{ndof} \left(R^{\mathcal{T}_i}_{|_{S_k^{b_i}}}\right)_{lj} \overline{\mathbb{W}}_j^{\mathcal{T}_i}\,. \tag{38}$$

The L^2-error at the step n between the exact solution and the approximated solution is computed from values of V_x at $n\Delta t$ and σ_{xx} at $(n+\frac{1}{2})\Delta t$:

$$err^n_{\mathrm{L}^2} = \sqrt{\sum_{i=1}^{N} dx_i \left[\left(V_x(n\Delta t, x_i) - (V_x)_i^n\right)^2 \ +\ \left(\sigma_{xx}\left(\left(n+\frac{1}{2}\right)\Delta t, x_i\right) - (\sigma_{xx})_i^{n+1/2}\right)^2 \right]},$$

where N is the number of points on the line $y = 1.0$ and dx_i is the length of the i-th edge.

On the figures 3, 4, 5 and 6, we have displayed, firstly on the left, the numerical error in the L^2-norm in logarithmic scale by respect to the mesh step h, and secondly on the right, the numerical error in the L^2-norm in logarithmic scale as a function of the CPU time. The meshes are the same as those presented in the previous section except that unstructured meshes are composed of four Delaunay meshes of the unit square gathered together. This has been done to explicitly identify in the mesh the lines $x = 1$ and $y = 1$ in order to be able to calculate here the L^2-error on the line $y = 1$ without interpolation. The mesh step h is the longest edge of the mesh.

For solutions at times lower than 0.8 s, when the pulse is still completely inside the domain, as on the figures 3 and 4, we observe a second-order convergence on uniform meshes. On unstructured meshes, the order of accuracy depends of the choice of the degree of the polynomials since a third order convergence is observed for both P3 and P4 methods. Concerning the efficiency, if a given L^2-error is sought, the corresponding CPU time is always lower for the high order polynomials and for both type of meshes despite the fact that high-order methods necessitate lower time-steps and more degrees of freedom on each element. So, we can conclude that the high order approximation method is more accurate and more efficient.

On the other hand, for solutions at times greater than 0.8 s, when the pulse reaches the boundary and goes out of the domain, as on figures 5 and 6 presenting solutions at time $t = 1.0$ s, we observe that the order of

convergence is one for all the methods except the finite volume (P0) method when structured meshes are used. On the other hand, for unstructured meshes, we remark a second-order convergence. These differences between solutions, at times $t = 0.4$ s and $t = 1.$ s, come from the absorbing condition which is not accurate enough, especially when high degree polynomials are employed. The properties of such absorbing conditions are quite known : results are not very accurate in presence of grazing waves and for too small numerical domains for which the boundaries are rapidly reached by the waves. Extension of such absorbing conditions to high order is not obvious, particularly in three dimensions of space. A way to improve the results consists in surrounding the domain by Perfectly Matched Layers (PML), initially developed for the Maxwell equations by Bérenger [3]. Many variations of this method have been proposed. Among them, we can quote the convolutional Perfectly Matched Layer (C-PML) proposed by Komatitsch and Martin [15] for three-dimensional elastodynamic equations which, compared to other methods, do not necessitate any splitting of the unknowns. We are interested now in the implementation of such conditions.

Lastly, we remark than the results obtained using unstructured meshes are very satisfactory even better as those of structured meshes. It is probably due to the choice of Delaunay meshes which have well known properties. Indeed, each Delaunay mesh has, for example, local orthogonality properties with its dual mesh, called Voronoï mesh, whereas the only characteristic of structured meshes is periodicity.

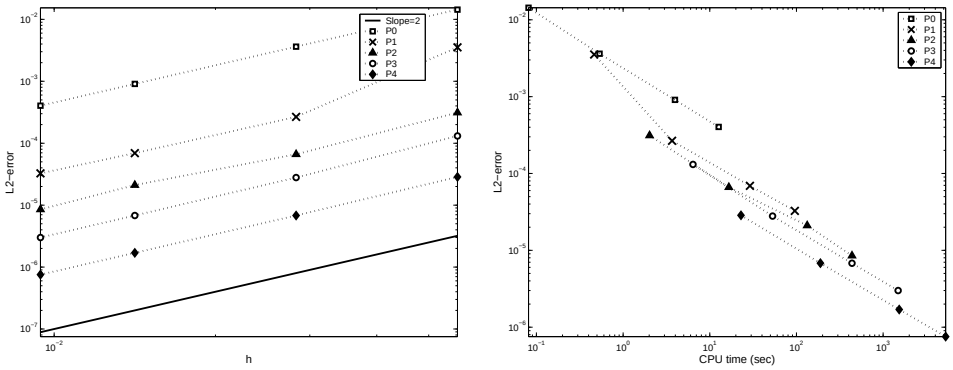

FIGURE 3. Convergence and CPU time on uniform meshes at $t = 0.4$ when the wave is inside the domain.

5.3. **Propagation of an eigenmode in 3D**

The last test case concerns the propagation of an eigenmode in three dimensions of space. The domain of computation is the unit cubic cavity on which we apply free surface boundary conditions. We are interested in the $(1, 1, 1)$ mode whose exact solution is given by:

$$\left\{\begin{array}{rcl} V_x &=& \cos(\pi x)\ (\sin(\pi y) - \sin(\pi z))\ \cos(\Omega t)\,, \\ V_y &=& \cos(\pi y)\ (\sin(\pi z) - \sin(\pi x))\ \cos(\Omega t)\,, \\ V_z &=& \cos(\pi z)\ (\sin(\pi x) - \sin(\pi y))\ \cos(\Omega t)\,, \\ \sigma_{xx} &=& -A\ \sin(\pi x)\ (\sin(\pi y) - \sin(\pi z))\ \sin(\Omega t)\,, \\ \sigma_{yy} &=& -A\ \sin(\pi y)\ (\sin(\pi z) - \sin(\pi x))\ \sin(\Omega t)\,, \\ \sigma_{zz} &=& -A\ \sin(\pi z)\ (\sin(\pi x) - \sin(\pi y))\ \sin(\Omega t)\,, \\ \sigma_{xy} &=& \sigma_{xz} = \sigma_{xz} = 0\,, \end{array}\right. \tag{39}$$

with $A = \sqrt{2\,\rho\,\mu}$ and $\Omega = \pi\sqrt{\frac{2\mu}{\rho}}$. As previously, we set $\rho = 1.0$, $\lambda = 0.5$ and $\mu = 0.25$, and the initialisation of the leap-frog scheme is realized by taking the values at $t = 0$ for the velocity components and at $t = \frac{\Delta t}{2}$ for the

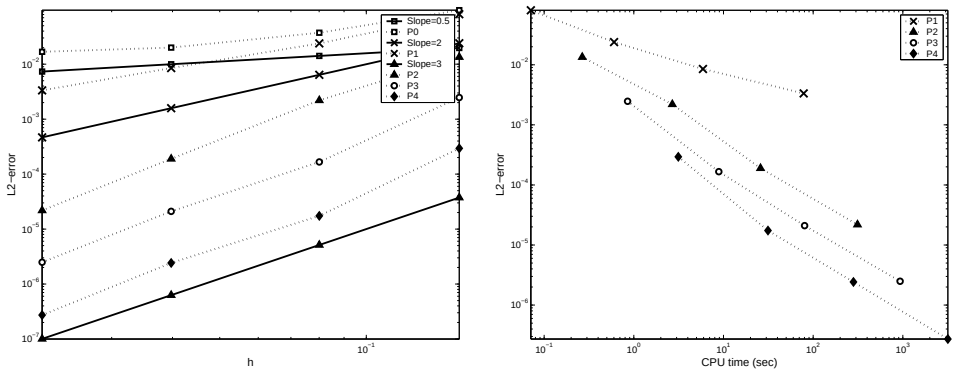

FIGURE 4. Convergence and CPU time on unstructured meshes at $t = 0.4$ when the wave is inside the domain.

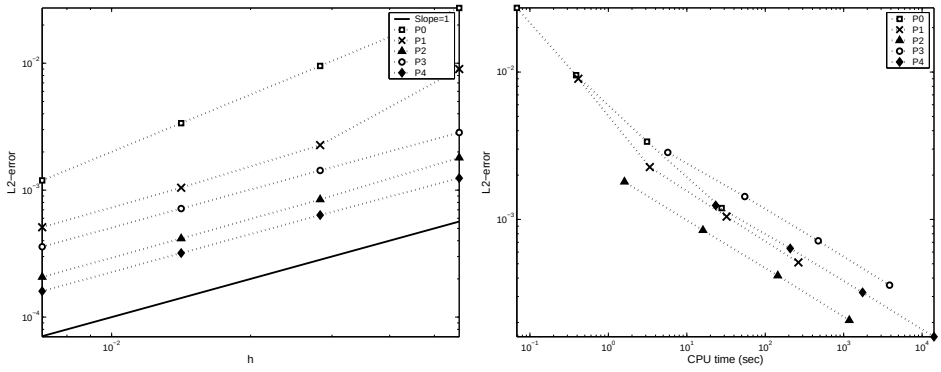

FIGURE 5. Convergence and CPU time on uniform meshes at $t = 1.0$ when the wave is outgoing.

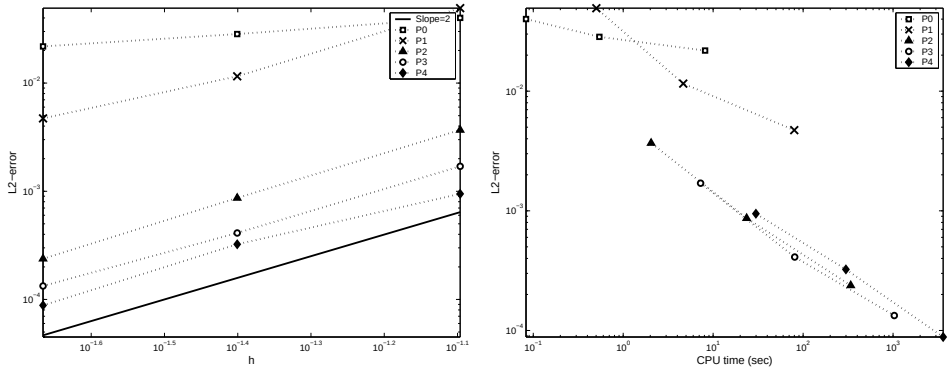

FIGURE 6. Convergence and CPU time on unstructured meshes at $t = 1.0$ when the wave is outgoing.

components of the stress from the analytical expressions (39). The L^2-error at the step n between the exact solution and the approximated solution in the unit cube depends on the velocities V_α ($\alpha = x, y, z$) at $n\Delta t$ and

the stress $\sigma_{\alpha\beta}$ $(\alpha, \beta = x, y, z)$ at $(n + \frac{1}{2})\Delta t$:

$$err^n_{\mathrm{L}^2} = \sqrt{\sum_{i=1}^{N_T} \int_{\mathcal{T}_i} \left[\sum_{\alpha\in\{x,y,z\}} (V_\alpha(n\Delta t, x_i) - (V_\alpha)^n_i)^2 + \sum_{\alpha,\beta\in\{x,y,z\}} \left(\sigma_{\alpha\beta}\left(\left(n+\frac{1}{2}\right)\Delta t, x_i\right) - (\sigma_{\alpha\beta})^{n+1/2}_i \right)^2 \right]}.$$

As in 2D, structured and unstructured meshes have been used. Structured meshes are obtained by dividing the domain in cubic cells which are split in six tetraedra. The unstructured meshes are Delaunay meshes constructed by a mesher from 2D surfacic Delaunay meshes of the boundaries of the domain. The mesh step h is here also the length of the longest edge of the mesh.

On the figures 7 and 8, we display, on the left the numerical error in L^2-norm in logarithmic scale by respect to the mesh step h. On the right of these figures, we represent the numerical error in L^2-norm in logarithmic scale by respect to the CPU time. We observe a second-order convergence on uniform meshes and on unstructured meshes, the accuracy increases with the order of the method. The convergence order is about $k+1$ for a method based on polynomials of degree k. This superconvergence is only possible because, as in the two dimensional case, the unstructured meshes possess nice properties. More, the free surface condition is accurately discretized compared to the absorbing condition. If we examine the efficiency, we notice that, to obtain a given L^2-error, methods based on high order polynomials need lower CPU times. So, we can conclude that higher order approximations are more accurate and more efficient for both type of meshes.

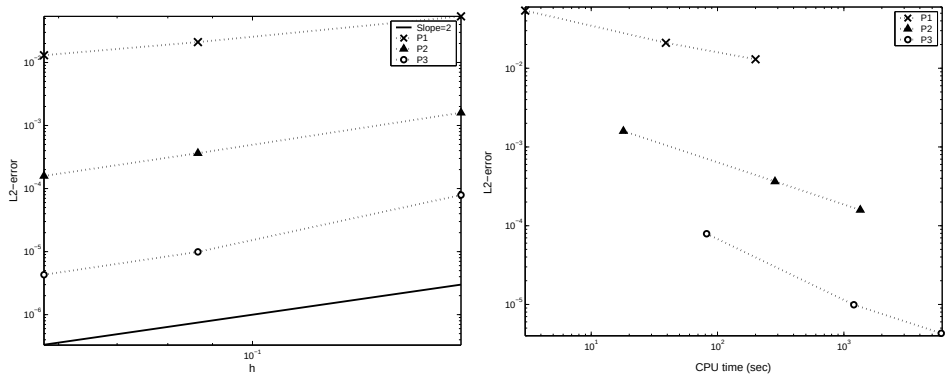

FIGURE 7. Convergence and CPU time for the (1,1,1) eigenmode at $t = 5.0$ on uniform meshes. (computations on 8 processors)

6. Conclusion

We proposed a Discontinuous Galerkin method to solve the elastodynamic equations, written in velocity-stress formulation, in two and three dimensions of space. This non-diffusive method relies on a centered scheme in space and a leap-frog scheme in time. Studying the discrete energy of the system, we proved that it is preserved by the method on an infinite domain. More, the scheme is stable under a CFL-type condition. Stability and convergence are numerically studied via several computations in two and three dimensions of space. Globally, the results are similar to those obtained for the Maxwell equations. The main conclusions of this study are the accuracy and the efficiency of the method particularly for higher orders polynomials. The free surface boundary condition is accurately approximated. On the contrary, the absorbing boundary condition could be improved, by introducing Perfectly Matched Layers. Results are also dependent on the quality of the mesh, the

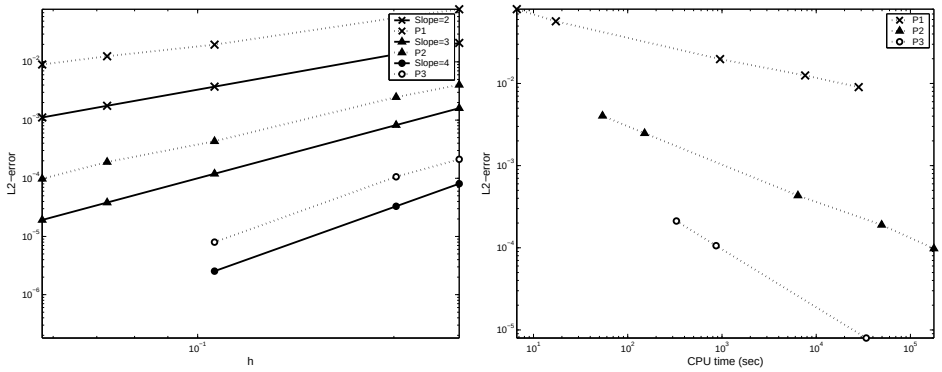

FIGURE 8. Convergence and CPU time for the (1,1,1) eigenmode at $t = 5.0$ on unstructured meshes.

unstructured Delaunay meshes providing better results as simple structured meshes. Now, we will be interested in simulations of more realistic problems including point (explosion or point-dislocation) or extended (dynamic non-planar crack rupture) sources and complex media. Moreover, some studies on high-order leap-frog schemes are in progress in order to improve accuracy in time.

REFERENCES

[1] M. BENJEMAA, N. GLINSKY-OLIVIER, V.M. CRUZ-ATIENZA, J. VIRIEUX AND S. PIPERNO, *Dynamic non-planar crack rupture by a finite volume method*, Geophys. J. Int., 171, pp 271–285, 2007.

[2] M. BENJEMAA, *Etude et simulation numérique de la rupture dynamique des séismes par des méthodes d'éléments finis discontinus*, Ph.D. thesis Nice-Sophia Antipolis University, 2007.

[3] J.-P. BÉRENGER, *A perfectly matched layer for absorption of electromagnetic waves*, Journal of Computational Physics, 114, pp 185–200, 1994.

[4] N. CANOUET, L. FEZOUI AND S. PIPERNO, *A Discontinuous Galerkin method for 3D Maxwell's equation on non-conforming grids*, Sixth Conference on Mathematical and Numerical Aspects of Wave propagation, G.C. Cohen Ed., Springer, Finland, pp 389–394, 2003.

[5] B. COCKBURN AND C. SHU, *The local Discontinuous Galerkin method for time dependent convection-diffusion systems*, SIAM J. Numer. Anal., 35, pp 2440–2463, 1998.

[6] B. COCKBURN, G. KARNIADAKIS AND C. SHU, *Discontinuous Galerkin Methods*, Theory, Computation and Applications, Lect. Notes Comput. Sci. Eng. 11, Springer, Berlin, 2000.

[7] L. DEMKOWICZ AND J. KURTZ, *Projection-based interpolation and automatic hp-adaptivity for finite element discretizations of elliptic and Maxwell problems*, ESAIM: proceedings, 21, pp 1–15, 2007.

[8] M. DUMBSER AND M. KÄSER, *An arbitrary high-order Discontinuous Galerkin method for elastic waves on unstructured meshes II: the three-dimensional isotropic case*, to appear in Geophysical J. Int.

[9] L. FEZOUI, S. LANTERI, S. LOHRENGEL AND S. PIPERNO, *Convergence and stability of a Discontinuous Galerkin time-domain method for the 3D heterogeneous Maxwell equations on unstructured meshes*, M2AN, 39 (6), pp 1149–1176, 2005.

[10] K.O. FRIEDRICHS, *Symmetric positive linear differential equations*, Comm. Pure Appl. Math., 11, pp 333–418, 1958.

[11] C. JOHNSON AND J. PITKÄRANTA, *An analysis of the Discontinuous Galerkin method for a scalar hyperbolic equation*, Math. Comp., 46, pp 1–26, 1986.

[12] C. JOHNSON, U. NÄVERT AND J. PITKÄRANTA, *Finite element methods for linear hyperbolic equations*, Comput. Methods Appl. Mech. Engrg., 45, pp 285–312, 1984.

[13] M. KÄSER AND M. DUMBSER, *An arbitrary high-order Discontinuous Galerkin method for elastic waves on unstructured meshes I: the two-dimensional isotropic case with external source terms*, Geophysical J. Int., 166 (2), pp 855-877, 2006.

[14] D. KOMATITSCH AND J.P. VILOTTE, *The spectral-element method: an efficient tool to simulate the seismic response of 2D and 3D geological structures*, Bull. Seism. Soc. America, 88 (2), pp 368–392, 1998.

[15] D. KOMATITSCH AND R. MARTIN, *An unsplit convolutional Perfectly Matched Layer improved at grazing incidence for the seismic wave equation*, Geophysics, 72 (5), pp SM155–SM167, 2007.

[16] P. LESAINT, *Sur la résolution des systèmes hyperboliques du premier ordre par des méthodes d'éléments finis*, Ph.D. thesis, University of Paris VI, 1975.

[17] P. Lesaint and P.-A. Raviart, *On a finite element method for solving the neutron transport equation*, in Mathematical Aspects of Finite Element Methods in Partial Differential Equations, C.A. deBoor, ed., Academic Press, New York, pp 89–123, 1974.

[18] W. Reed and T. Hill, *Triangular mesh methods for the neutron transport equation*, Technical Report LA-UR-73-479, Los Alamos Scientific Laboratory, Los Alamos, NM, 1973.

[19] M. Remaki, Méthodes numériques pour les équations de Maxwell instationnaires en milieu hétérogène, Ph.D. thesis ENPC CERMICS, France, 1999.

[20] S. Piperno, M. Remaki and L. Fezoui, *A non-diffusive finite volume scheme for the 3D Maxwell equations on unstructured meshes*, SIAM J. Numer. Anal., 39, pp 2089–2108, 2002.

[21] E. Süli, C. Schwab and P. Houston, *hp-DGFEM for partial differential equations with non-negative characteristic form*, in Discontinuous Galerkin Methods Theory, Computation and Applications, Lect. Notes Comput. Sci. Eng. 11, B. Cockburn, G.E. Karniadakis and C.-W. Shu eds., Springer, Berlin, pp 221–230, 2000.

[22] J. Virieux, *P-SV wave propagation in heterogeneous media, velocity-stress finite difference method*, Geophysics, 51, pp 889–901, 1986.

[23] K.S. Yee, *Numerical solution of initial boundary value problems involving Maxwell's equations in isotropic media*, IEEE Trans. Antennas and Propagat., 14 (3), pp 302–307, 1966.